Modeling of a Counter Flow Plate Fin Heat Exchanger

Ruoxu Jia[1], Junling Hu[*1], Xingguo Xiong[2]
[1]Department of Mechanical Engineering, University of Bridgeport, Bridgeport, CT 06604 USA
[2]Department of Electrical and Computer Engineering, University of Bridgeport, Bridgeport, CT 06604 USA
*jjhu@bridgeport.edu

Abstract: Heat exchangers are used widely in many industries for heat recovery or cooling purposes. This paper simulated a counter flow pate fin parallel heat exchanger. A representative repeating unit cell of the multi-channeled heat exchanger was taken as the computational domain, which includes a cold channel and a hot channel separated by plates. Hot oil and cold water entered two separate parallel channels in opposite directions. The detailed distributions of temperature, velocity, and pressure were used to analyze the performance of the heat exchanger. A parametric study of channel length is also conducted to see its effect on heat transfer effectiveness and pressure drop.

Keywords: Plate fin heat exchanger, CFD, heat transfer

1. Introduction

Currently, heat exchangers have a wide range of industry applications. They are widely used in space heating, refrigeration, power plants, petrochemical plants, petroleum refineries and sewage treatment [1]. There are many types of heat exchanger designs for various applications. The major types of heat exchanger include double pipe, shell-tube, plate and shell, plate fin, and phase change heat exchangers. The flow in a heat exchanger can be arranged as parallel flow, counter flow, and cross flow. New heat exchangers have been designed for emerging thermal engineering fields, such as miniaturized heat exchanger for cooling electronics components and systems, miniaturized heterogeneously catalyzed gas-phase reactions, thermoelectric generators, etc. [2-5]. New materials, such as polymers, have been explored to develop polymer heat exchangers for better fouling and corrosion resistance [6].

Parallel-plated heat exchangers have been studied analytically and experimentally to provide formulations for heat exchanger design. Vera and Linan [3] analyzed multilayered, counter flow, parallel-plate heat exchangers numerically and theoretically. They developed a two-dimensional model to find analytical expressions and their approximations for the fully developed laminar counter flow in long parallel-plate heat exchangers. Kragh et al. [7] developed a new counter flow heat exchange for ventilation systems in cold climates. The efficiency of the new heat exchanger was calculated theoretically and measured experimentally.

Zhan et al. [8] used an experimentally validated model to understand the influence of operational and geometric parameters of the cross-flow and counter-flow exchangers on the different metrics of cooling performance. Overall the counter-flow exchanger demonstrated better cooling effectiveness and higher cooling capacity than the cross-flow system. However, the energy efficiency of the counter-flow system is often seen to be lower than that of the more conventional cross-flow dew point system [8]. The shape of the cross section of the heat exchanger also has a significant effect on efficiency. Hasan et al. [9] studied the effect of channel geometry on the performance of a counter-flow MCHE (main cryogenic heat exchanger). The influences of channel shapes such as circular, square, rectangular, isotriangular, and trapezoidal were evaluated by numerical simulations. In their studies, decreasing the volume of each channel or increasing the number of channels increased the heat transfer, but the required pumping power and pressure drop were also increased. The channel with a circular shape resulted in the best overall performance [10].

Recently, CFD analysis of heat exchanger has been used to help design heat exchangers and to analyze their thermal performance, effectiveness and temperature distributions. This paper simulated the heat transfer and fluid flow in a multilayered counter flow plate fin heat exchanger. The temperature distributions and heat transfer rate are analyzed to study the performance of the heat exchanger.

2. Governing Equations

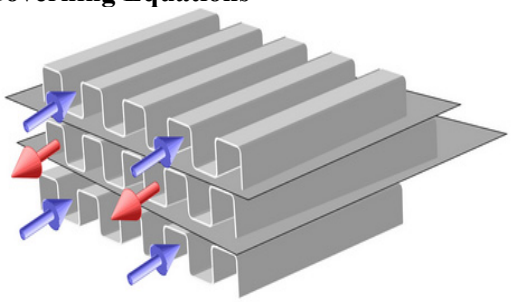

Figure 1. Schematic of a counter flow plate fin heat exchanger [11]

Figure 1 shows a schematic sketch of a multilayered counter flow plate fin heat exchanger. Hot and cold fluids marked with red and blue colors in Fig. 1 enter numerous channels in separate layers. Each channel is formed by a thin folded plate and separation plates between cold and hot fluids. The thickness of the plates is t and the channels have a square shape with a size w and length L. A unit cell consists of a cold channel and a hot channel is taken as the computational domain for CFD analysis, as shown in Fig. 2.

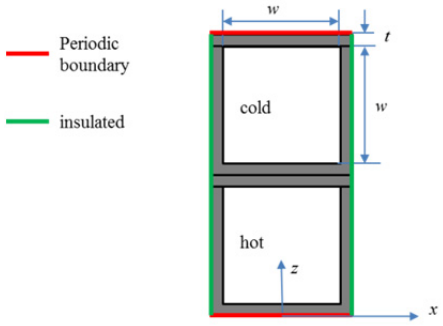

Figure 2. Side view of the computational domain consisting of one cold and one hot channel

For a laminar flow in the channels, Navier-Stokes equations are solved for the heat transfer and fluid flow in the channels. The mathematical model includes conservations of mass, momentum and energy in the fluid domains and conduction in the solid domain for a steady state laminar flow.

Mass conservation

$$u\frac{\partial u}{\partial x}+v\frac{\partial u}{\partial y}+w\frac{\partial u}{\partial z}=0$$

Momentum conservation

$$u\frac{\partial u}{\partial x}+v\frac{\partial u}{\partial y}+w\frac{\partial u}{\partial z}=\frac{\mu}{\rho}\left(\frac{\partial^2 u}{\partial x^2}+\frac{\partial^2 u}{\partial y^2}+\frac{\partial^2 u}{\partial z^2}\right)-\frac{1}{\rho}\frac{\partial p}{\partial x}$$

$$u\frac{\partial v}{\partial x}+v\frac{\partial v}{\partial y}+w\frac{\partial v}{\partial z}=\frac{\mu}{\rho}\left(\frac{\partial^2 v}{\partial x^2}+\frac{\partial^2 v}{\partial y^2}+\frac{\partial^2 v}{\partial z^2}\right)-\frac{1}{\rho}\frac{\partial p}{\partial y}$$

$$u\frac{\partial w}{\partial x}+v\frac{\partial w}{\partial y}+w\frac{\partial w}{\partial z}=\frac{\mu}{\rho}\left(\frac{\partial^2 w}{\partial x^2}+\frac{\partial^2 w}{\partial y^2}+\frac{\partial^2 w}{\partial z^2}\right)-\frac{1}{\rho}\frac{\partial p}{\partial z}+\mathrm{g}$$

Energy conservation

$$u\frac{\partial T}{\partial x}+v\frac{\partial T}{\partial y}+w\frac{\partial T}{\partial z}=\frac{k}{\rho c_p}\left(\frac{\partial^2 T}{\partial x^2}+\frac{\partial^2 T}{\partial y^2}+\frac{\partial^2 T}{\partial z^2}\right)$$

where u, v, and w are velocity components in x, y, z direction, respectively; ρ is density, μ is dynamic viscosity, p is pressure , T is the temperature , g is gravitational acceleration, k is thermal conductivity, and c_p is heat capacity

Hot fluid and cold fluids enters channels of the opposite side. Velocity inlet boundary conditions are taken at the inlets and pressure outlet boundary are set at the fluid exits. The boundary conditions for walls are set as shown in Fig. 2. Two side walls are insulated due to symmetry. The periodic boundary condition is set for the top and bottom walls.

3. Numerical model

This paper simulated a plate fin heat exchanger with oil and water as two working fluids. Oil at 330K enters the hot channel with an inlet velocity of 0.005 m/s. Water at 300K enters the cold channel with an inlet velocity of 0.02 m/s. Both channels have a square cross section with dimensions of 2 cm × 2 cm. The channel length is varied from 20 cm to 120 cm in a parametric study. The channel wall thickness is 1 mm. Tables 1-3 listed the material properties and other important parameters used in this simulation. The properties of oil and water were set as a function of temperature in the simulation. They vary with temperature significantly in the calculation. However, the properties of water at 300K and those of oil at 330K were listed in Tables 2 and 3 to calculate some important parameters for the understanding of the heat transfer and fluid flow in the channels and also compare with theoretical results. The important parameters [12] include:

Prandtl number $P_r=\frac{C_p\mu}{k}$

Reynolds number $Re=\frac{\rho V D_h}{\mu}$

hydrodynamic entrance length $L_h=0.05ReD_h$

thermal entrance length $L_t = P_r L_h$
heat capacity rate $C = \rho V A C_p$
capacity ratio $c = \frac{C_{min}}{C_{max}}$
maximum heat transfer rate:
$\dot{Q}_{max} = C_{min}(T_{max} - T_{min})$

Table 1. Channel dimensions and steel properties

Parameter	Symbol	Value	unit
Channel length	L	0.2 to 1.2	m
Channel width	W	0.02	m
Channel thickness	t	0.001	m
Density	ρ_s	7850	kg/m^3
Thermal conductivity	k_s	44.5	W/m·K
Heat capacity	c_{ps}	475	J/kg·K

Table 2. Properties and simulation conditions of oil

Parameter	Symbol	Value	unit
Density	ρ_o	875.7	kg/m^3
Thermal conductivity	k_o	0.141	W/m·K
Heat capacity	c_{po}	2034.6	J/kg·K
Dynamics viscosity	μ	0.0855	Kg/m·s
Prandtl numberl	Pr_o	1235	
Inlet velocity	V_{ino}	0.005	m/s
Reynolds number	Re_o	1.01	
Inlet temperature	T_{inO}	330	K
Heat capacity rate	C_o	3.52	W/K
Maximum heat transfer rate	$\dot{Q}_{max}$	106	W
Hydrodynamic entrance length	L_h	0.001	m
Thermal entrance length	L_t	1.25	m

Table 3. Properties and simulation conditions of water

Parameter	Symbol	Value	unit
Density	ρ_w	997.7	kg/m^3
Thermal conductivity	k_w	0.606	W/m·K
Heat capacity	c_{pw}	4182	J/kg·K
Dynamics viscosity	μ	8.54×10^{-4}	Kg/m·s
Prandtl number	Pr_w	5.90	
Inlet velocity	V_{inw}	0.02	m/s
Reynolds number	Re_w	467	
Inlet temperature	T_{inw}	300	K
Heat capacity rate	C_w	33.4	W/K
Capacity ratio	c	0.106	
Hydrodynamic entrance length	L_h	0.467	m
Thermal entrance length	L_t	2.76	m

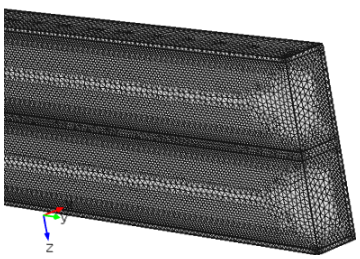

Figure 3. Computational mesh

The conjugate heat transfer problem was solved using the Heat Transfer module of COMSOL 4.3b. An unstructured mesh of tetrahedral elements as shown in Fig. 3 is used for each simulation. The numbers of elements varies from 794k to 1080k when the channel length increases from 0.2m to 1.2m. The simulations were carried out in a laptop with Intel core i7 processors and 8 GB RAM. Each simulation took 38 minutes to over an hour to get a solution. Finer meshes near the wall boundaries are generated to resolve the high velocity and temperature gradients at the near wall boundaries. A structured mesh stretched in fluid direction could be used to significantly reduce the number of mesh and thus solution time, however, the General Projection function in COMSOL does not work with the structured mesh. The General Projection function is used to find the average fluid temperature along the channel direction.

4. Results

Figures 4 and 5 report the temperature distribution at the surface of the 3D computational domain and in the x-z planes sections along the channel length direction. It can be clearly seen that hot oil enters the top channel with a uniform temperature of 330K and is cooled along the channel length and cold water enters the top channel with a temperature of 300K and is heated along the channel length. Heat transfer between the two channels are through the channel walls. As shown in Fig. 6, heat spreads over the walls and the walls serve as a media to exchange heat with fluids.

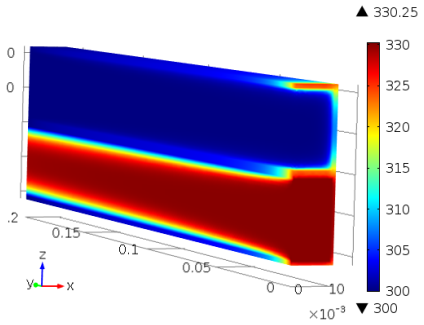

Figure 4. Surface temperature at the channels surfaces and walls

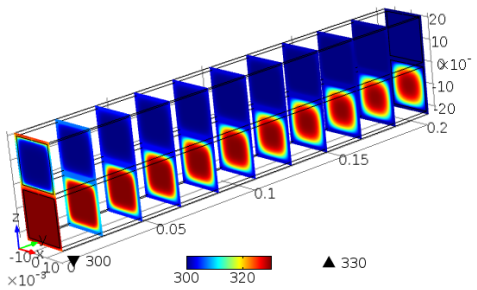

Figure 5. Temperature fields in the x-z cut-planes along the channel length.

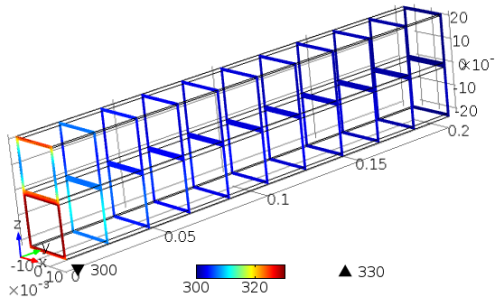

Figure 6. Temperature fields in the solid walls in the x-z cut-planes along the channel length

The average channel fluid temperatures along the channel length direction are shown in Figure 7. The General Projection functions have been used to project the three-dimensional temperature fields to one dimensional average temperature along the channel length direction. The average temperature drop for the oil is higher than that of water as a much higher heat capacity rate is used for water. Increasing the channel length from 0.2 m to 1.2 m, the oil is further cooled significantly and water temperature has no significant increase. The average temperatures of hot and cold fluids at channel exits are shown in Fig. 8.

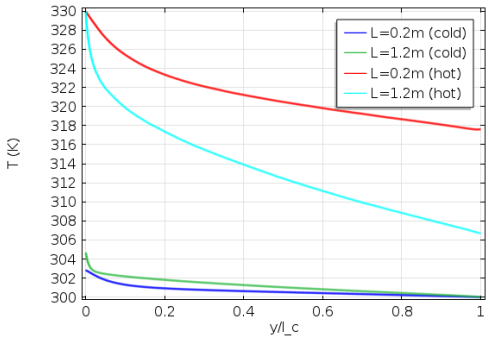

Figure 7. Average fluid temperatures in hot and cold channels along the channel length

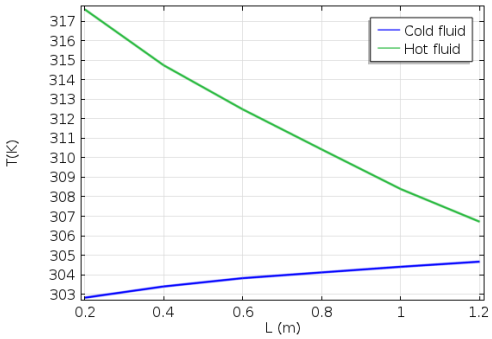

Figure 8. Average fluid temperature at the channel exits vs channel length

The heat transfer effectiveness of a heat exchanger is defined as the ratio of the actual heat transfer rate over the maximum heat transfer rate,

$$\varepsilon = \frac{\dot{Q}}{\dot{Q}_{\max}}$$

where the maximum heat transfer rate is calculated as the heat capacity rate of oil multiplied by the temperature difference of the inlet temperatures. The calculated heat transfer effectiveness is plotted in Figure 9. Further extending the channel length will increase the heat transfer effectiveness, but at a lower increase rate.

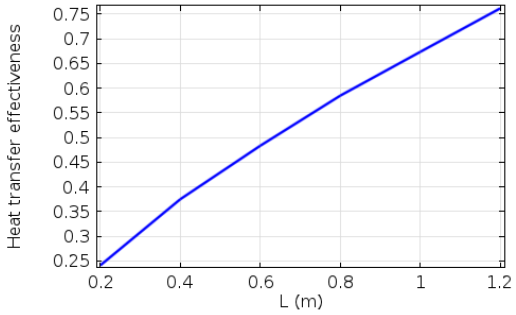

Figure 9. Heat transfer effectiveness obtained with various channel length

Figures 10 to 12 show the centerline temperature and the normalized centerline velocity in the hot and channels. The centerline velocities show that fluid in the hot channel reaches a fully developed state very quickly at the entrance, which is close to the theoretical value of 0.001m for the hydrodynamic entrance length. The approximate thermal entrance length can also be calculated to be 1.25 m by $L_t = P_r L_h$. Prandtl number is defined as the ratio of momentum diffusivity to thermal diffusivity of fluid. Heat diffuses very slowly compared to momentum diffusion in high Prandtl number fluids, which

result in a thinner thermal boundary layer relative to the velocity boundary layer and a longer thermal entrance length. As the Prandtl number of oil is in the range of in a range of 1220-6185 in the hot channel, the velocity boundary layer is fully developed while the temperature boundary is not fully developed shown in Figure 11. The change of velocity after hydrodynamic entrance length is due to the variation of thermal physical properties with temperature.

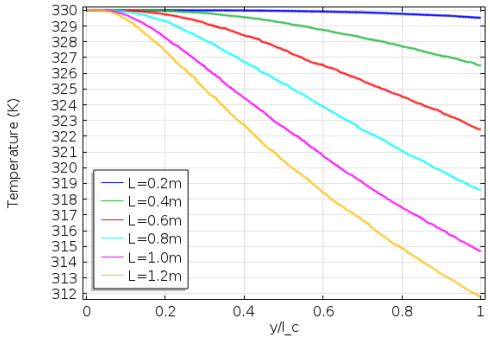

Figure 10. Fluid temperature along hot channel centerline

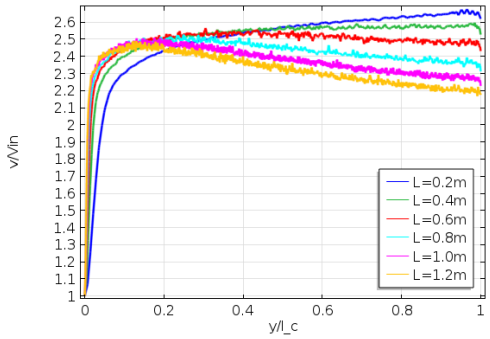

Figure 11. Streamwise velocity along hot channel centerline

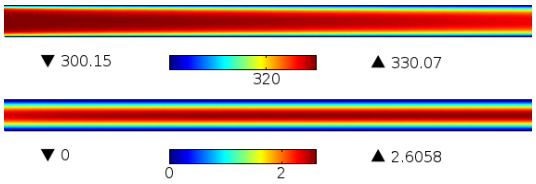

Figure 12. Temperature field (top) and normalized streamwise velocity (v/V_{in}) field (bottom) in the hot channel for the case of L = 0.4 m

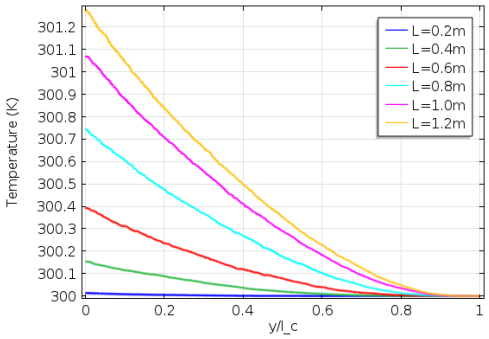

Figure 13. Fluid temperature along cold channel centerline

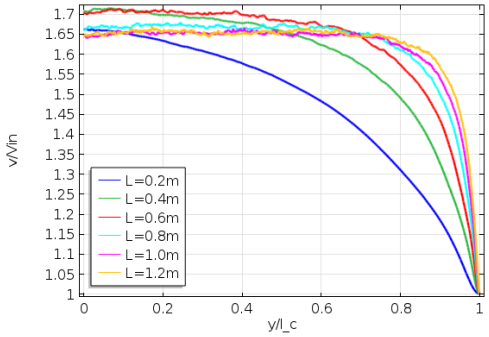

Figure 14. Streamwise velocity along cold channel centerline

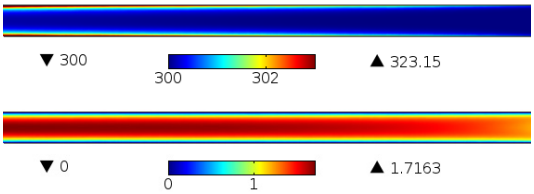

Figure 15. Temperature field (top) and normalized streamwise velocity (v/V_{in}) field (bottom) in the cold channel for the case of L = 0.4 m

The Prandtl number of water varies in a range of 3.6-5.90 in the cold channel. The centerline temperatures in Figure 13 show that the temperature boundary layer in the cold channel has not reached a fully developed state, even when the channel length is 1.2m. Figure 14 shows the velocity boundary layer reaches the fully developed state around 0.4m. Figure 15 confirms that the temperature boundary layers are far from fully developed and the velocity boundary layers are close to fully developed at the end of the channel with a length of 0.4m. They are in agreement with the approximate hydrodynamic entrance length (L_h = 0.47 m) and

thermal entrance length (L_h = 2.76 m) calculated in Table 3.

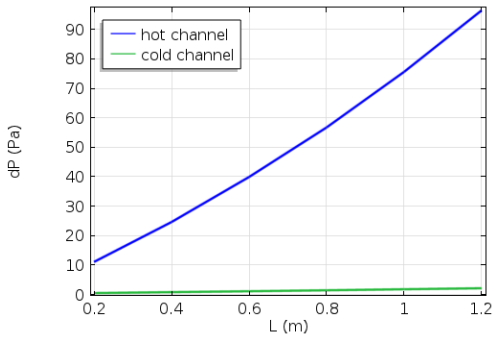

Figure 16. Pressure drop in the hot and cold channels

The pressure drops in the hot and cold channels are plotted in Figure 16. Pressure drop increases about proportionally with the increase of channel length as the hydrodynamic entrance is small compared to the channel length. The pressure drop in the hot channel is about 50 time of the pressure drop in the cold channel as the viscosity of oil is much higher than that of water. Therefore, a high flow rate of water can be used to increase heat transfer effectiveness without significantly increasing pressure drop. Further increasing the length of the channel can have higher heat transfer effectiveness, but will result in a higher pressure drop and also a big size heat exchanger.

5. Conclusions

In this study, a 3D model of a counter flow plate fin heat exchanger was developed to simulate the heat transfer and fluid flow in a unit cell composed of one cold channel and one hot channel. The model was simulated in COMSOL 4.3b Heat Transfer module with oil and water as two working fluids. The detailed temperature and velocity distributions are presented for a better understanding of the heat transfer phenomena in a heat exchanger. The hydrodynamic and thermal entrance lengths are compared with the theoretical results and good agreement are found. A parametric study was conducted to show the effect of channel length on the temperature distribution, heat transfer effectiveness, and pressure drop. The established model can be further developed to optimize a heat exchanger with similar geometry.

6. References

1. S. Kakac and H. Liu, Heat Exchangers: Selection, *Rating and Thermal Design*, 2nd ed, CRC Press, (2002).
2. A.E. Quintero, M. Vera and B. Rivero-deAguilar, Wall conduction effects in laminar counterflow parallel-plate heat exchangers, *International Journal of Heat and Mass Transfer*, **70**, pp. 939-953 (2014).
3. M. Vera and A. Linan, Laminar counterflow parallel-plate heat exchangers: exact and approximate solutions, *International Journal of Heat and Mass Transfer*, **53**, pp. 4885-4898 (2010).
4. J. Esarte, G. Min, D.M. Rowe, Modelling heat exchangers for thermoelectric generators, *J. Power Sources*, **93**, pp. 72-76 (2001).
5. D.B. Tuckerman, R.F.W. Pease High-performance heat sinking for VLSI IEEE Elect. *Device Lett.*, **2**, pp. 126‑129 (1981),.
6. J. Yu, and H.Zhao, A numerical model for thermoelectric generator with the parallel-plate heat exchanger, *J. Power sources*, **172**, pp. 428-434 (2007).
7. J. Kragh, J. Rose, T.R. Nielsen, and S. Svendsen, New counter flow heat exchanger designed for ventilation systems in cold climates, *Energy and Buildings*, **39**, pp. 1151-1158 (2007).
8. Changhong Zhan, Zhiyin Duan, Xudong Zhao, Stefan Smith, Hong Jin, and Saffa Riffat, Comparatie study of the performance of the M-cycle counter-flow and cross-flow heat exchangers for indirect evaporative cooling-paving the path toward sustainable cooling of buildings, *Energy*, **36**, pp 6790-6805 (2011).
9. M.I. Hasan, A.A. Rageb, M. Yaghoubi, H. Homayoni Influence of channel geometry on the performance of a counter flow microchannel heat exchanger, *Int. J. Therm. Sci.,* **48**, pp. 1607‑1618 (2009).
10. Tsung-Lin Liu, Ben-Ran Fu, Chin Pan, Boiling heat transfer of co- and counter-current microchannel heat exchangers with gas heating, *International Journal of Heat and Mass Transfer*, **56**, pp. 20–29 (2013).
11. http://thisisecs.com/blog/2008/11/04/heat-transfer/
12. Yunus Cengel and Afshin Ghajar, *Heat and mass transfer: fundamentals and applications*, McGraw-Hill Science/Engineering/Math, 4th edition, (2010).